Published in final edited form as:
Exp Hematol. 2010 July ; 38(7): 593–602. doi:10.1016/j.exphem.2010.04.008.

Amelioration of a Mouse Model of Osteogenesis Imperfecta with Hematopoietic Stem Cell Transplantation: Micro-Computed Tomography Studies

Meenal Mehrotra[a,b], **Michael Rosol**[c,d], **Makio Ogawa**[a,b,d], and **Amanda C. LaRue**[a,b,d,*]

[a] Research Services, Department of Veterans Affairs Medical Center, Charleston, SC

[b] Department of Pathology and Laboratory Medicine, Medical University of South Carolina

[c] Department of Radiology and Radiological Science, Medical University of South Carolina

[d] Hollings Cancer Center, Medical University of South Carolina

Abstract

Objective—To test the hypothesis that hematopoietic stem cells (HSCs) generate bone cells using bone marrow (BM) cell transplantation in a mouse model of osteogenesis imperfecta (OI). OI is a genetic disorder resulting from abnormal amount and/or structure of Type I collagen and is characterized by osteopenia, fragile bones and skeletal deformities. Homozygous OI murine mice (*oim*; B6C3Fe *a/a-Col1a2*^{oim}/J) offer excellent recipients for transplantation of normal HSCs, because fast turnover of osteoprogenitors has been shown.

Methods—We transplanted BM mononuclear cells or 50 BM cells highly enriched for HSCs from transgenic enhanced green fluorescent protein (EGFP) mice into irradiated *oim* mice and analyzed changes in bone parameters using longitudinal Micro-Computed Tomography (micro-CT).

Results—Dramatic improvements were observed in 3D micro-CT images of these bones 3 to 6 months post-transplantation when the mice showed high levels of hematopoietic engraftment. Histomorphometric assessment of the bone parameters such as trabecular structure and cortical width supported observations from 3D images. There was an increase in bone volume, trabecular number and trabecular thickness with a concomitant decrease in trabecular spacing. Analysis of a non-engrafted mouse or a mouse that was transplanted with BM cells from *oim* mice showed continued deterioration in the bone parameters. The engrafted mice gained weight and became less prone to spontaneous fractures while the control mice worsened clinically and eventually developed kyphosis.

Conclusions—These findings strongly support the concept that HSCs generate bone cells. Furthermore, they are consistent with observations from clinical transplantation studies and suggest therapeutic potentials of HSCs in OI.

[*]Corresponding Author: Dr. Amanda C. LaRue, PhD, Department of Veterans Affairs Medical Center, 109 Bee Street, Charleston, SC 29401-5799, Tel (843) 789-6712, Fax (843) 876-5381; laruerc@musc.edu.

Conflict of Interest Disclosure

The authors declare that they have no conflict of interest.

Keywords

Stem Cell Transplantation; Hematopoietic Stem Cells; Osteogenesis Imperfecta; Micro-Computed Tomography; Bone

Introduction

Osteogenesis imperfecta (OI) or brittle bone disease is an autosomal dominant disorder caused by a mutation in one of the 2 genes that encode type I collagen, COL1AI or COL1A2, the primary structural protein of bone. It is the most common hereditary bone disease and is characterized by mild to severe reduction in the quantity of bone matrix that leads to repeated fractures and bone deformities including metaphyseal flaring and thin diaphysis [1]. Normal bone responds to fracture or loading by increasing bone resorption and formation [2]. In a similar way, the OI bone initiates a cycle of bone remodeling in an attempt to form a stronger matrix. A high bone turnover rate has been documented, especially in severe forms of OI [3] [4]. Given this high turnover, it is feasible that the deleterious effects in OI could be reduced or neutralized by the presence of normal osteoprogenitor cells. It has been observed that marrow stromal cells delivered via the circulatory system can migrate to and become incorporated into the bone in mice [5] [6]. Based on this concept, transplantation studies with normal bone marrow (BM) cells have been performed in a limited number of children with severe OI [7] [8] [9]. Even though the number of patients was small, these studies suggested beneficial clinical effects of BM transplantation for OI, including increase in total bone mineral content, growth speed and a reduced frequency of fracture.

While studies by Horowitz, et al. point to the BM as a potential therapeutic source of osteoprogenitors, the cell within the BM capable of giving rise to these cells remains unclear. Current dogma suggests that BM contains two types of stem cells, hematopoietic stem cells (HSCs) and mesenchymal stem cells (MSCs), and that their repertoire of differentiation/reconstituting potentials are distinct and separate from each other. HSCs produce blood cells while MSCs are thought to generate a number of mesenchymal cells including fibroblasts, adipocytes, chondrocytes and osteocytes [10]. However, studies have begun to question the distinction between the potentials of HSCs and MSCs. Reports have demonstrated that transplantation of 3000 side population (SP) cells that are highly enriched for HSCs generated osteoblasts *in vivo* [11]. Likewise, Dominici, et al. [12] transplanted marrow cells that had been transduced with GFP-expressing retro-viral vector and observed a common retro-viral integration site in clonogenic hematopoietic cells and osteoprogenitors from each of the recipient mice. Using a transplantation model in which the BM of lethally irradiated recipient mice is reconstituted by a clonal population of cells derived from a single enhanced green fluorescent protein ($EGFP^+$) HSC, we have documented that many types of tissue fibroblasts/myofibroblasts are derived from the HSC (reviewed in [13]). Recently, we have also demonstrated *in vitro* and *in vivo* that adipocytes are of HSC origin [14]. Collectively, these studies suggest that HSCs may be able to give rise to mesenchymal tissues.

In the present study, we used a mouse model of OI (*osteogenesis imperfecta murine; oim*) and tested the hypothesis that HSC transplantation would improve clinical pathologies in animals with OI. We transplanted $EGFP^+$ mononuclear cells (MNCs) or purified HSCs from EGFP mice into irradiated *oim* mice and analyzed changes in bone parameters using longitudinal Micro-Computed Tomography (micro-CT). The results demonstrate dramatic improvements in bone parameters, including bone volume, trabecular number and thickness, cortical width and bone density of the transplanted *oim* mice relative to control *oim* mice, suggesting the utility and feasibility of HSC transplantation as a therapy for OI.

Material and methods

Mice

Breeding pairs of transgenic EGFP$^+$ mice (C57BL/6) [15] were kindly provided by Dr. Okabe (Osaka University, Japan). These mice ubiquitously express EGFP under the control of the actin promoter and were used as BM donors. Homozygous OI mice (*oim*; B6C3Fe a/a-Col1a2^{oim}/J) were purchased from Jackson Labs, Bar Harbor, ME. This mouse model has been shown to have a phenotype similar to that seen in human type III OI, including a decreased body size, abnormal bone mineralization (contributing to the brittleness of the bones), decreased bone density and a fragile skeleton susceptible to fractures. While the skeleton becomes progressively deformed with age, homozygous mice can live a normal life span. All mice were bred and maintained at the Animal Research Facility of the Veterans Affairs Medical Center. All aspects of animal research have been conducted in accordance with guidelines set by the PHS Policy on Humane Care and Use of Laboratory Animals and the Institutional Animal Care and Use Committee of the Department of Veterans Affairs Medical Center.

Reagents

For use in negative immuno-magnetic selection, purified antibodies to B220/CD45R (RA3-6B2), Gr-1/Ly-6C (RB6-8C5), TER-119 (TER-119), Mac-1/CD11b (M1/70), CD4/L3T4 (GK-1.5), CD8/Ly-2 (53.6.7) were purchased from BD Pharmingen (San Diego, CA). The Dynabeads® sheep anti-rat IgG beads were purchased from Invitrogen Dynal AS (Carlsbad, CA). Antibodies used for cell sorting including phycoerythrin (PE)-conjugated anti-Sca-1 (D7), allophycocyanin (APC)-conjugated anti-c-kit (2B8), biotin-conjugated lineage panel antibodies (B220, Gr-1, CD3ε, TER-119, Mac-1) and streptavidin-conjugated APC-Cy-7 were purchased from BD Pharmingen. Biotinylated anti-CD34 (RAM34) was purchased from eBiosciences (San Diego, CA). Appropriate isotypes were also purchased from BD Pharmingen. PE-conjugated antibodies used for multi-lineage hematopoietic engraftment including B220/CD45R (RA3-6B2), Thy-1.2/CD90.2 (30-H12), Mac-1/CD11b (M1/70) and Gr-1/Ly-6G and Ly-6c (RB6-8C5) were purchased from BD Pharmingen.

Cell Preparation

Ten to fourteen-week-old EGFP mice were used as donors. BM cells were flushed from tibiae and femurs of euthanized mice, pooled and washed with phosphate-buffered saline (PBS) containing 0.1% bovine serum albumin (BSA). MNCs were isolated by gradient separation using Lympholyte-M (Cedarlane Laboratories Limited, Ontario, Canada). For transplantation of BM cells that are highly enriched for HSCs, the MNCs were further processed for lineage-negative (Lin$^-$) cells by negative selection using antibodies to B220, Gr-1, CD4, CD8, TER-119, Mac-1 and Dynabeads® sheep anti-rat IgG beads. Candidate HSCs were identified by staining the resulting Lin$^-$ cells with PE-conjugated anti-Sca-1, APC-conjugated anti-c-kit, biotinylated anti-CD34 and biotinylated lineage panel antibodies (B220, Gr-1, CD3ε, TER-119, Mac-1) followed by streptavidin-conjugated APC-Cy7. The cells were then resuspended at 1×10^6/ml in Ca^{2+}-, Mg^{2+}- free Hanks balanced salt solution (HBSS; Invitrogen, Gaithersburg, MD) containing 2% fetal bovine serum (FBS; Atlanta Biologicals, Norcross, GA), 10mM HEPES, 1% penicillin/streptomycin and Hoechst 33342 (Sigma, St. Louis, MO; 5μg/ml) and incubated at 37°C for 60 min [16] [17]. The cells were then washed, stained with propidium iodide (1 μg/mL), resuspended in PBS with 0.1% BSA, and kept on ice until sorting. Cell sorting was performed using a MoFlo Cell Sorter (DakoCytomation, Fort Collins, CO). Appropriate isotype-matched controls were analyzed. The gates used for side population (SP) cells corresponded to R3 and R4 fractions of Goodell, et al. [18] and R1 and R2 populations of Matsuzaki, et al. [19]. Purified Lin$^-$ Sca-1$^+$ c-kit$^+$ CD34$^-$ SP cells were sorted and kept on ice until transplantation.

Transplantation

Five-month old *oim* mice were used as recipients for MNC transplantation, and 3-month old *oim* mice for HSC transplantation. All the recipient *oim* mice were scanned by micro-CT before transplantation to obtain baseline images. Recipient *oim* mice were given a single 800-cGy dose of total-body irradiation using a 4×10^6 V linear accelerator. Either 2×10^5 MNCs or 50 Lin^- $Sca\text{-}1^+$ $c\text{-}kit^+$ $CD34^-$ SP cells prepared from the EGFP mice were injected via tail vein into the irradiated *oim* mice. The mice transplanted with 50 Lin^- $Sca\text{-}1^+$ $c\text{-}kit^+$ $CD34^-$ SP cells also received injection of 2×10^5 un-manipulated BM cells from an *oim* mouse which served as radio-protective cells during the post radiation pancytopenia period. A transplanted *oim* mouse which showed no engraftment and an irradiated *oim* mouse transplanted with 2×10^5 MNCs from another *oim* mouse were used as controls. After transplantation, the mice were fed an irradiated breeder's diet (Tekland Global Diets, Harlan Labs) and milliQ water *ad libitum*. Neomycin was added to the water in the first month after transplantation to prevent infection. The mice were followed for 6 months after transplantation. For analysis of hematopoietic engraftment, peripheral blood (PB) was obtained from the retro-orbital plexus or the tail vein of the recipient mice at 3–6 months after transplantation. Red blood cells were lysed with PharM Lyse (BD Pharmingen). Donor-derived $EGFP^+$ cells in T cell, B cell, granulocyte and monocyte/macrophage lineages were analyzed by staining with PE-conjugated anti-Thy-1.2, anti-CD45R/B220 and a combination of anti-Gr-1 and anti-Mac-1, respectively. We performed the analysis of hematopoietic engraftment using a FACSCalibur (Becton Dickinson, San Jose, CA).

Micro-CT Analysis

Micro-CT scanning allows nondestructive analysis of bone architecture at the trabecular level, both qualitatively by visual inspection of three-dimensional (3D) images of the trabecular network, and quantitatively by calculation of model-independent 3D morphometric parameters. *In vivo* scanning of small animals allows longitudinal measurement of local architectural changes of the bone in the same animal over time [20]. High-resolution (18 micrometer on-a-side cubic voxels) micro-CT images were obtained from live mice under isoflurane anesthesia using the Siemens Inveon micro-CT scanner (Siemens Medical Solutions, Knoxville, TN). Mice were positioned on a movable bed and imaged with a bone mineral tissue density phantom within the scan field of view. The scan field of view encompassed only the hindlimbs, minimizing radiation dose to the body of the animal. Importantly, it has been established that radiation doses to mice with micro-CT scans are well below the lethal dose for mice [21]. Each acquired image set was composed of 203 individual projections with 6.5-s exposure time per projection. After acquisition, each raw data set was reconstructed using the Siemens software package IRW and Cobra EXXIM software (EXXIM Computing, Livermore, CA), implementing the modified Feldkamp filtered backprojection algorithm (Shepp-Logan filter) with isotropic 18.29 μm^3 reconstructed voxel size, which resulted in an image matrix size of 1024 × 1024 × 1536 pixels [22]. Two-dimensional axial and 3D images were reconstructed for qualitative and quantitative analyses. For region of interest (ROI) measurement and analyses, axial images were displayed using the 2- and 3D biomedical image analysis software package (CT Bone Visualization and Analysis, Siemens Medical Solutions, Knoxville, TN). Axial reformats were performed to allow slice-by-slice, manual tracing of the contours of the cortical and trabecular bone. For cross-sectional study of trabecular bone, a region of 183 μm^2 was analyzed approximately 250 μm below the growth plate, while cortical bone width was measured in an equivalent area of 183 μm^2 in the diaphysis approximately 4500 μm from the growth plate. The analysis gave information about the main histomorphometric parameters including bone volume, trabecular number, thickness and spacing and cortical width. The bone mineral density within the region was also determined. Information about the trabecular pattern factor was also obtained. Trabecular pattern factor is a relationship between the convex and the concave surfaces wherein the convex surfaces are

more numerous in disconnected structures while the concave surfaces are abundant in well-connected surfaces. Consequently trabecular pattern factor is low in well-connected bone and high where highly disconnected trabeculae are observed [23] [24].

Results

Improvement in bone parameters after MNC transplantation

Six months after transplantation of MNCs, the levels of hematopoietic engraftment in 2 mice were 50% and 94%, respectively. Micro-CT images of distal femur and proximal fibula/tibia from the mouse with 94% engraftment taken before and 6 months after transplantation are shown in Figure 1. Panels A and B show images of the femur, fibula and tibia respectively, of the *oim* mouse prior to transplantation and Panels D and E the same structures at 6 months post-transplantation. These images document dramatic improvements in the bone architecture both in the femur and tibia. Macroscopically, improved bone structure can be appreciated in the femur (compare Panels A and D), while new bone formation was observed in the tibia as evidenced by the filling of previously observed gaps (compare Panels B and E). Calcification was observed in the patellar tendon (Panel D, asterisk). Regions of interest for histomorphometric analysis were similar in all data sets. In this analysis, improvements were seen in both trabecular bone architecture and the cortical bone width after transplantation (compare Panels C and F).

Morphometric analysis of the data obtained before transplantation, at 3 months and at 6 months post-transplantation is presented in Table 1. Continuous improvement was noted in all parameters. Most striking, bone volume of both femur and tibia increased 2.5-fold in 6 months with transplantation. The trabecular number doubled with an increase in trabecular thickness and a concomitant decrease in trabecular spacing, which illustrates betterment of the trabecular architecture. Cortical width showed approximately 20 and 40% increase in femur and tibia, respectively. An increase in the trabecular and cortical bone densities was also observed. There was a 63% decrease in the trabecular pattern factor in tibia and a 71% decrease in the femur at 6 months post-transplantation, indicating an improvement in trabecular connectivity and structure.

The mouse with 50% engraftment also showed similar results after transplantation (images not shown). There was a 62% increase in the bone volume, a 30% increase in the trabecular thickness, a 24% increase in the trabecular number with a 35% decrease in the trabecular spacing. The trabecular pattern factor decreased 49% while the cortical thickness increased about 60%. A substantial increase in the trabecular and cortical bone densities was also observed at 6 months post transplantation.

Exacerbation of bone parameters in a non-engrafted mouse

One mouse injected with MNCs from EGFP mice showed complete absence of hematopoietic engraftment at 3 and 6 months after transplantation and provided an excellent non-engraftment control. In contrast to the dramatic improvements seen in the engrafted mice, the bone parameters in this mouse continued to deteriorate over the 6 month time period. The gaps in the bone structure seen in femur, fibula and tibia at 0 time point became more prominent 6 months later (Figure 2, Panels A, B, C and D). Cross-sectional analysis shows that there was a loss of trabecular bone architecture (Panels C and F). These observations were supported by morphometric analysis showing decreases in bone volume, trabecular number, trabecular thickness and cortical width and increase in trabecular spacing (Table 2). The trabecular pattern factor increased from 5.66 to 16.22 in tibia and 34.81 to 44.45 in femur, indicating that the connectivity of the trabeculae becomes worse. The density of the trabecular and the cortical bones essentially did not change over the time period.

Improvement in bone parameters following HSC transplantation

We next transplanted 50 Lin^{-}, c-kit^{+}, $Sca\text{-}1^{+}$, $CD34^{-}$, SP cells into irradiated *oim* mice to determine the role of HSCs in the etiology and the potential therapy for OI. Flow cytometric analysis of PB cells from the mouse is shown in Figure 3. $EGFP^{+}$ cells represented approximately 72% of the total cells. The images of distal femur and proximal fibula/tibia are shown in Figure 4. An improvement in the bone architecture can be appreciated by comparing the images of the femur, fibula and tibia before transplantation (Panels A, B and C) with the images taken 6 months after transplantation (Panels D, E and F). Interestingly, as seen in the mouse transplanted with MNCs, calcification was observed in the patellar tendon (Panel D, asterisk). Cross-sectional analysis showed improvement in both trabecular bone architecture and cortical bone width. Morphometric analyses of the tibia before transplantation and at 3 and 6 months post-transplantation are presented in Table 3(A). Notably, at 6 months post-transplantation, there were higher than 30% increases in bone volume, trabecular thickness and cortical width. There were little changes in the trabecular number and spacing. There was a 27% increase in the trabecular bone density, but no change was observed in the cortical bone density. Trabecular pattern factor showed a 62% decrease in the tibia at 6 months post transplantation, indicating an improvement in the connectivity and structure of the trabeculae.

Deterioration of bone parameters in a mouse transplanted with oim BM cells

An additional control consisting of an *oim* mouse transplanted with MNCs from an *oim* mouse showed a steady deterioration in the bone architecture over the 6 month period in all bones analyzed (Figure 5). Loss of bone stability is suggested by the shift in the position of patella at 6 months (Panels A and D, asterisk). Morphometric analysis of the tibia shown in Table 3 (B) illustrates the most substantial decrease in trabecular number (43%) accompanied by an extensive increase in trabecular spacing. While trabecular thickness and density increased slightly, there were 32% decrease in bone volume and 20% decrease in cortical bone width. Similar to the other control mouse (Table 2) the cortical density showed no change.

Discussion

In this brief report, we present evidence that the transplantation of normal HSCs provides long-term amelioration of the bone abnormalities in the *oim* mouse model. We transplanted irradiated *oim* mice with either BM MNCs or 50 BM cells from transgenic EGFP mice that were highly enriched for HSCs and carried out longitudinal micro-CT analysis of the femur, fibula and tibia of the recipient mice. Dramatic improvements observed in the 3D micro-CT images of these bones 3 to 6 months post-transplantation, correlated with high levels of hematopoietic engraftment and corresponded to improvements in histomorphometric parameters. Analysis showed an increase in bone volume, trabecular number, thickness and density and a decrease in trabecular spacing. Decrease in trabecular pattern factor indicated an improvement in the connectivity and structure of the trabeculae. In addition to quantifiable improvements in the bone architecture, we also observed clinical improvements in the engrafted *oim* mice. The weight of the mice increased over the course of the experiment, perhaps in part due to the dramatic improvements in the bone architecture and density. The mice also became more active and were less prone to fractures during routine bedding changes and animal husbandry. In contrast to the mice engrafted with normal HSCs, the bone architecture in the control mice continued to deteriorate over the course of the experiment. Clinically, the weight of the control mice decreased and the mice became sluggish and remained prone to fractures. They also exhibited marked dorsal kyphosis as has been reported in these mice with increasing age [25].

There have been few reports of transplantation studies using mouse models of OI. Studies by Wang, et al. [26] and Li, et al. [27] showed that the transplanted cells undergo osteoblastic

differentiation, deposit matrix and form bone *in vivo*. In these studies, the graft cells had been cultured before transplantation and the durations of the observation were 4 weeks or shorter. Because the cultured cells expressed low levels of Runx-2 under basal conditions, the bone engrafting cells were considered to be committed osteoprogenitors [27]. More recently, Dominici, et al. [28], using a different OI mouse model, studied long-term effects of transplantation of retrovirally GFP-labeled non-adherent BM cells. While hematopoietic engraftment persisted for 12 months the number of GFP-labeled bone cells declined to almost nil by the end of 52 weeks. No assessment of bone parameters or clinical effects of the transplantation was discussed in their paper.

Our observations in an OI mouse model are in agreement with the reports of clinical BM transplantation in children with the severe form of OI. In the first trial, three children with OI were transplanted with un-manipulated BM cells from sibling donors [7]. Three months after osteoblast engraftment, biopsied trabecular bone specimens showed evidence of new bone formation. There was an increase in the total body bone mineral content associated with increase in growth speed and reduced frequency of fractures [7]. Similar results were seen in an additional study with five children with severe OI [8]. With extended follow-up, the patients' growth rates either slowed down or plateaued, but bone mineral content continued to increase, suggesting a durable engraftment of osteogenic donor cells. Interestingly, when gene marked donor mesenchymal cells were used to treat six children with severe OI, enhancement in growth velocities was observed without increase in the total body bone mineral content [9]. Findings presented in this brief report together with the clinical observations by Horwitz, et al. [7] [8] [9] suggest therapeutic potentials of HSCs in OI. Studies are under way to confirm the donor HSC origin of the osteogenic cells in transplanted *oim* mice and to determine the mechanisms by which HSCs affect structural and clinical improvements in the OI model. These studies will unequivocally establish the origin of bone cells in HSCs as well as their use in the therapy of OI.

Acknowledgments

This work was supported by the Office of Research and Development, Medical Research Services, Department of Veterans Affairs (ACL) and by National Institutes of Health grant DK077821 (MO). The authors would like to acknowledge the Hollings Cancer Center Flow Cytometry Core and Small Animal Imaging Core with special thanks to Dr. Haiqun Zeng for assistance in FACS sorting and Raymond Chang for micro-CT scanning and assistance in analyzing the scan data. We would also like to thank the staff of the Radiation Oncology Department for assistance in irradiation of mice and the staff of the Ralph H. Johnson VA Medical Center Animal Facility for the care of mice. The authors would also like to thank Mr. Christopher Williams for his help during the transplantation experiments.

References

1. Shapiro JR, McBride DJ Jr, Fedarko NS. OIM and related animal models of osteogenesis imperfecta. Connective tissue research 1995;31:265–268. [PubMed: 15612365]
2. Raisz LG. Physiology and pathophysiology of bone remodeling. Clinical chemistry 1999;45:1353–1358. [PubMed: 10430818]
3. Baron R, Gertner JM, Lang R, Vignery A. Increased bone turnover with decreased bone formation by osteoblasts in children with osteogenesis imperfecta tarda. Pediatric research 1983;17:204–207. [PubMed: 6835724]
4. Rauch F, Travers R, Parfitt AM, Glorieux FH. Static and dynamic bone histomorphometry in children with osteogenesis imperfecta. Bone 2000;26:581–589. [PubMed: 10831929]
5. Pereira RF, O'Hara MD, Laptev AV, et al. Marrow stromal cells as a source of progenitor cells for nonhematopoietic tissues in transgenic mice with a phenotype of osteogenesis imperfecta. Proceedings of the National Academy of Sciences of the United States of America 1998;95:1142–1147. [PubMed: 9448299]

6. Hou Z, Nguyen Q, Frenkel B, et al. Osteoblast-specific gene expression after transplantation of marrow cells: implications for skeletal gene therapy. Proceedings of the National Academy of Sciences of the United States of America 1999;96:7294–7299. [PubMed: 10377408]
7. Horwitz EM, Prockop DJ, Fitzpatrick LA, et al. Transplantability and therapeutic effects of bone marrow-derived mesenchymal cells in children with osteogenesis imperfecta. Nature medicine 1999;5:309–313.
8. Horwitz EM, Prockop DJ, Gordon PL, et al. Clinical responses to bone marrow transplantation in children with severe osteogenesis imperfecta. Blood 2001;97:1227–1231. [PubMed: 11222364]
9. Horwitz EM, Gordon PL, Koo WK, et al. Isolated allogeneic bone marrow-derived mesenchymal cells engraft and stimulate growth in children with osteogenesis imperfecta: Implications for cell therapy of bone. Proceedings of the National Academy of Sciences of the United States of America 2002;99:8932–8937. [PubMed: 12084934]
10. Prockop DJ. Further proof of the plasticity of adult stem cells and their role in tissue repair. The Journal of cell biology 2003;160:807–809. [PubMed: 12642607]
11. Olmsted-Davis EA, Gugala Z, Camargo F, et al. Primitive adult hematopoietic stem cells can function as osteoblast precursors. Proceedings of the National Academy of Sciences of the United States of America 2003;100:15877–15882. [PubMed: 14673088]
12. Dominici M, Pritchard C, Garlits JE, Hofmann TJ, Persons DA, Horwitz EM. Hematopoietic cells and osteoblasts are derived from a common marrow progenitor after bone marrow transplantation. Proceedings of the National Academy of Sciences of the United States of America 2004;101:11761–11766. [PubMed: 15282377]
13. Ogawa M, LaRue AC, Drake CJ. Hematopoietic origin of fibroblasts/myofibroblasts: Its pathophysiologic implications. Blood 2006;108:2893–2896. [PubMed: 16840726]
14. Sera Y, LaRue AC, Moussa O, et al. Hematopoietic stem cell origin of adipocytes. Experimental hematology 2009;37:1108–1120. 1120, e1101–1104. [PubMed: 19576951]
15. Okabe M, Ikawa M, Kominami K, Nakanishi T, Nishimune Y. 'Green mice' as a source of ubiquitous green cells. FEBS letters 1997;407:313–319. [PubMed: 9175875]
16. Ebihara Y, Masuya M, Larue AC, et al. Hematopoietic origins of fibroblasts: II. In vitro studies of fibroblasts, CFU-F, and fibrocytes. Experimental hematology 2006;34:219–229. [PubMed: 16459190]
17. LaRue AC, Masuya M, Ebihara Y, et al. Hematopoietic origins of fibroblasts: I. In vivo studies of fibroblasts associated with solid tumors. Experimental hematology 2006;34:208–218. [PubMed: 16459189]
18. Goodell MA, Rosenzweig M, Kim H, et al. Dye efflux studies suggest that hematopoietic stem cells expressing low or undetectable levels of CD34 antigen exist in multiple species. Nature medicine 1997;3:1337–1345.
19. Matsuzaki Y, Kinjo K, Mulligan RC, Okano H. Unexpectedly efficient homing capacity of purified murine hematopoietic stem cells. Immunity 2004;20:87–93. [PubMed: 14738767]
20. Waarsing JH, Day JS, van der Linden JC, et al. Detecting and tracking local changes in the tibiae of individual rats: a novel method to analyse longitudinal in vivo micro-CT data. Bone 2004;34:163–169. [PubMed: 14751574]
21. Boone JM, Velazquez O, Cherry SR. Small-animal X-ray dose from micro-CT. Mol Imaging 2004;3:149–158. [PubMed: 15530250]
22. Ritman EL. Micro-computed tomography-current status and developments. Annual review of biomedical engineering 2004;6:185–208.
23. Hahn M, Vogel M, Pompesius-Kempa M, Delling G. Trabecular bone pattern factor--a new parameter for simple quantification of bone microarchitecture. Bone 1992;13:327–330. [PubMed: 1389573]
24. Dalle Carbonare L, Valenti MT, Bertoldo F, et al. Bone microarchitecture evaluated by histomorphometry. Micron 2005;36:609–616. [PubMed: 16242341]
25. Chipman SD, Sweet HO, McBride DJ Jr, et al. Defective pro alpha 2(I) collagen synthesis in a recessive mutation in mice: a model of human osteogenesis imperfecta. Proceedings of the National Academy of Sciences of the United States of America 1993;90:1701–1705. [PubMed: 8446583]

26. Wang X, Li F, Niyibizi C. Progenitors systemically transplanted into neonatal mice localize to areas of active bone formation in vivo: implications of cell therapy for skeletal diseases. Stem Cells 2006;24:1869–1878. [PubMed: 16675597]

27. Li F, Wang X, Niyibizi C. Distribution of single-cell expanded marrow derived progenitors in a developing mouse model of osteogenesis imperfecta following systemic transplantation. Stem Cells 2007;25:3183–3193. [PubMed: 17823236]

28. Dominici M, Marino R, Rasini V, et al. Donor cell-derived osteopoiesis originates from a self-renewing stem cell with a limited regenerative contribution after transplantation. Blood 2008;111:4386–4391. [PubMed: 18182575]

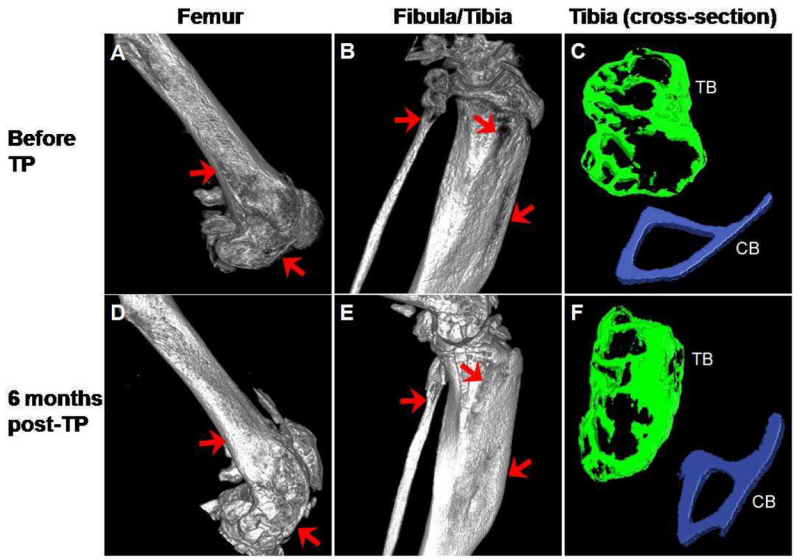

Figure 1.

Micro-CT images of femur, fibula and tibia from osteogenesis imperfecta murine (*oim)* mouse before and 6 months after transplantation of MNCs. Three-dimensional images are of the digitally reconstructed distal femur (**A**) and proximal fibula and tibia (**B**) from an *oim* mouse before transplantation and the images of the same areas (**D** and **E**, respectively) 6 months after transplantation. The irregular bone structures in the femur before transplantation (arrows, **A**) improved after transplantation (arrows, **D**) and calcification of the tendon attaching to the patella was noted after transplantation (asterisk, **D**). Gaps in the bone in the fibula and tibia (arrows, **B**) cannot be seen after transplantation (arrows, **E**). Comparison of the cross-sectional images of tibia before (**C**) and after (**F**) transplantation highlights the extensive improvement in both trabecular (TB; green) and cortical (CB; blue) bone. The images in A, B, D and E are shown at ~ 100% magnification, C and F are shown at ~ 290% magnification. Correlative images are all displayed using the same threshold values.

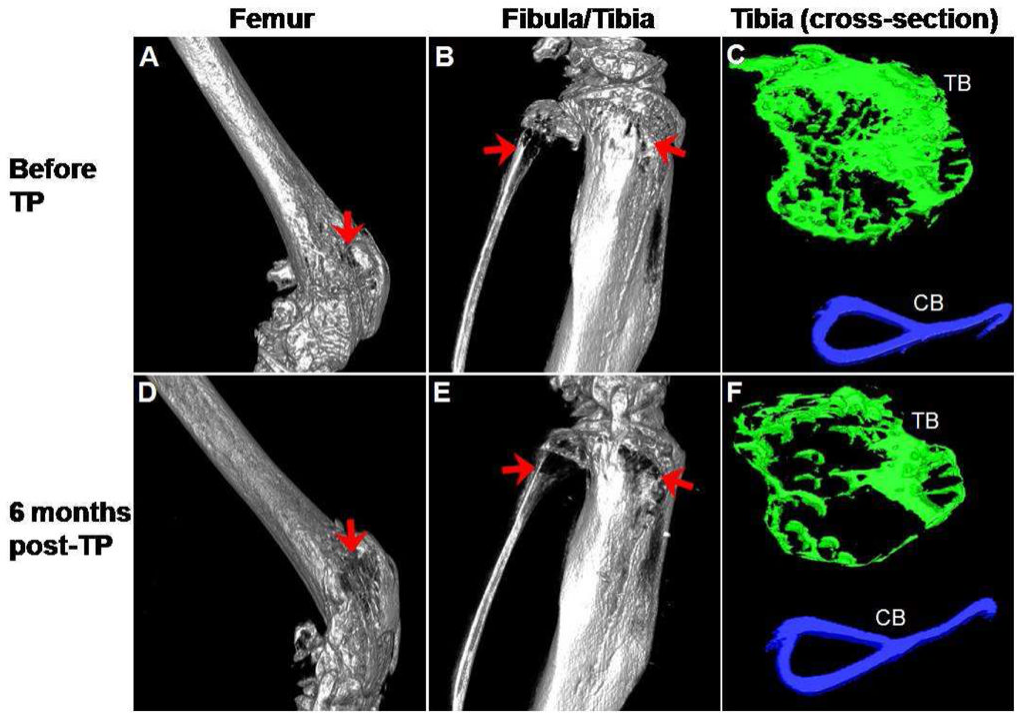

Figure 2.

Micro-CT images of femur and fibula and tibia from a non-engrafted osteogenesis imperfecta murine (*oim)* mouse. The irregular bone structure and gaps in the bone seen at initial imaging before transplantation (arrows, **A** and **B**) worsened 6 months later (**D** and **E**). Comparison of the cross-sectional tibial images before transplantation (**C**) and after 6 months (**F**) also showed marked loss in trabecular architecture. TB indicates trabecular bone and CB indicates cortical bone. The images in A, B, D and E are shown at ~ 100% magnification, C and F are shown at ~ 290% magnification. Correlative images are all displayed using the same threshold values.

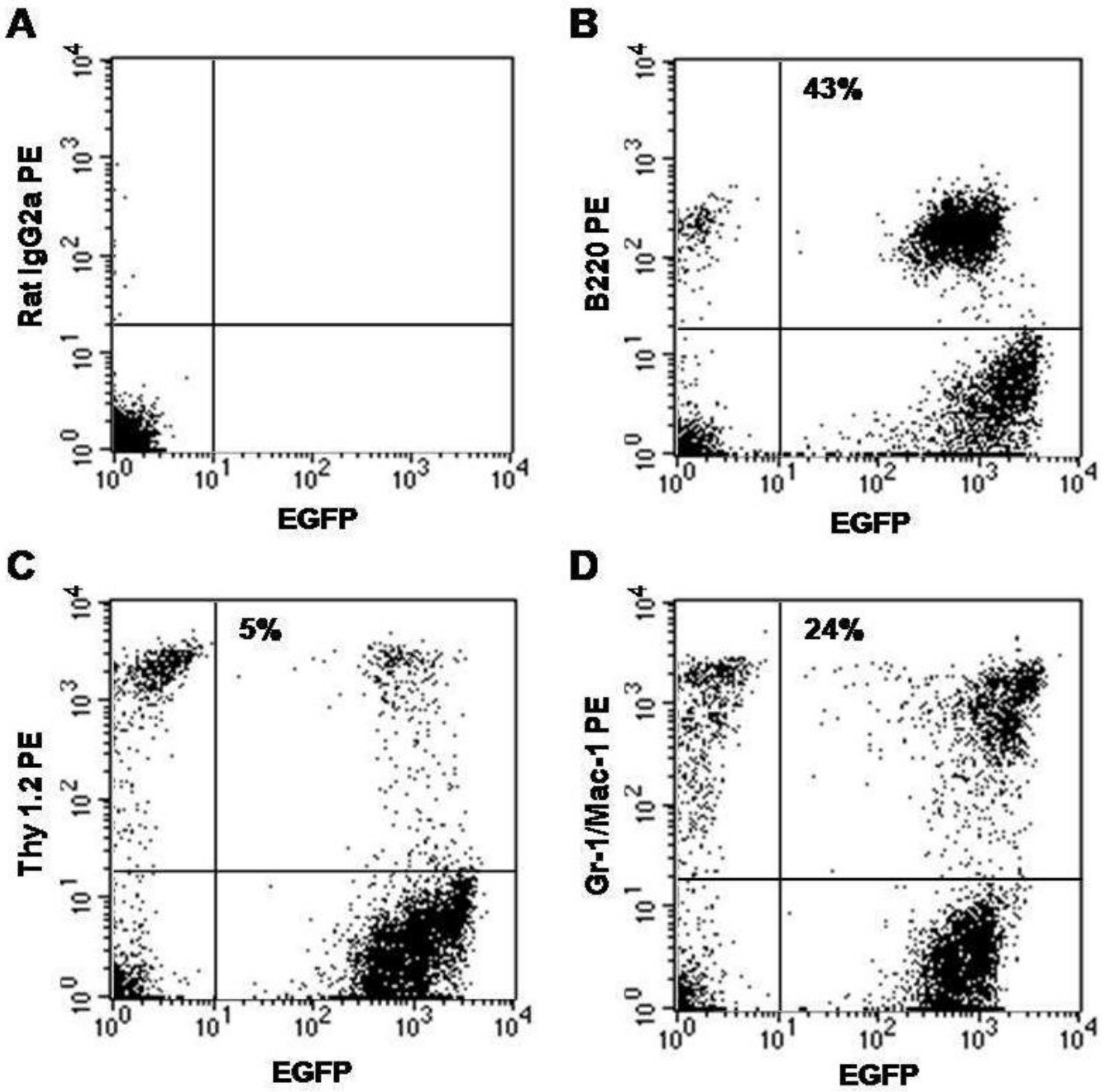

Figure 3.

Multilineage hematopoietic engraftment from transplantation of purified EGFP$^+$ HSCs. Shown is a flow cytometric analysis of nucleated cells from PB of a mouse 6 months after transplantation of 50 Lin$^-$ Sca-1$^+$ c-kit$^+$ CD34$^-$ SP cells. Isotype control is shown in (A). EGFP$^+$ cells represented 72% of total nucleated cells and consisted of 43% B-cells (B), 5% T-cells (C) and 24% granulocyte-macrophages (D).

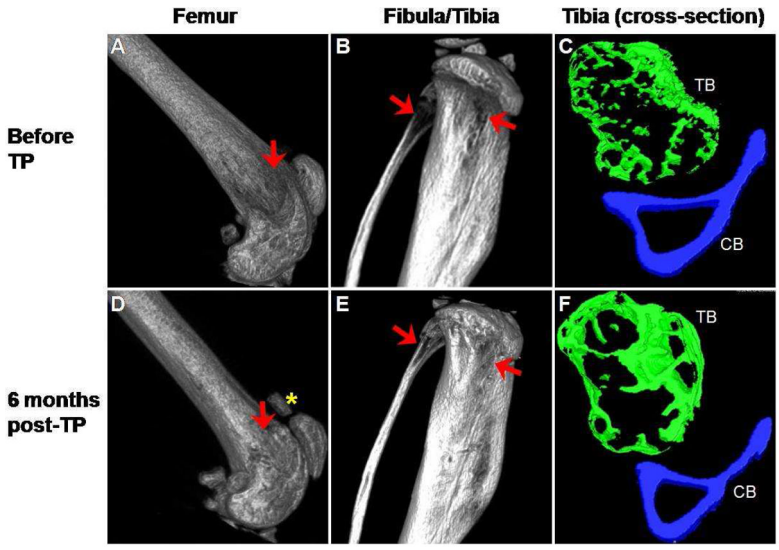

Figure 4.

Micro-CT images of femur, fibula and tibia from osteogenesis imperfecta murine (*oim)* mouse before and 6 months after transplantation of purified HSCs. The irregular bone structure in the femur before transplantation (arrow, **A**) improved after transplantation (arrow, **D**). Calcification of the tendon attaching to the patella was again noted after transplantation (asterisk, **D**). Similarly, the gaps in fibula and tibia (arrows, **B**) were filled after transplantation (arrows, **E**). Comparison of the cross-sectional images of tibia before (**C**) and after (**F**) transplantation highlights the extensive improvement in both trabecular (TB; green) and cortical (CB; blue) bone. The images in A, B, D and E are shown at ~ 100% magnification, C and F are shown at ~ 290% magnification. Correlative images are all displayed using the same threshold values.

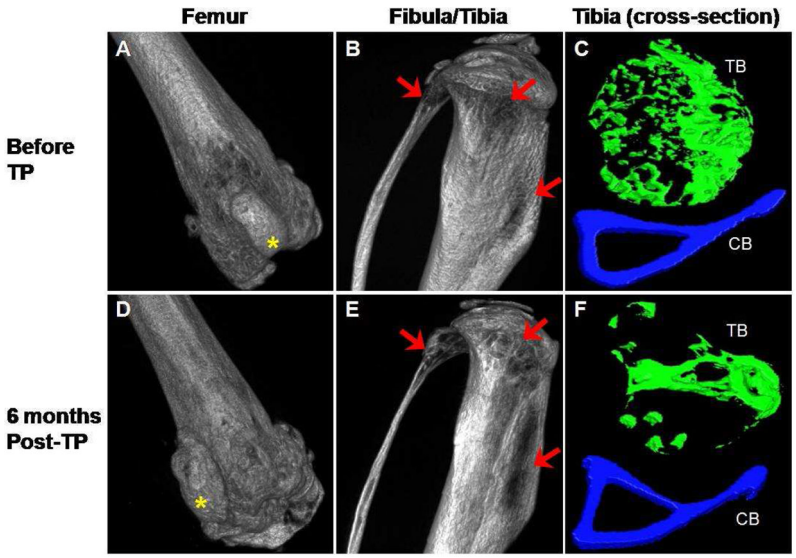

Figure 5.

Micro-CT images of distal femur and proximal fibula and tibia from an osteogenesis imperfecta murine (*oim)* mouse transplanted with BM cells from another *oim* mouse. The images are of the digitally reconstructed bones before (**A** and **B**) and 6 months after transplantation (**D** and **E**). The general worsening of the bone structure in the femur is exemplified by the loss of normal two-condyle structure of distal femur (**D**) and dislocation of the patella (asterisks in **A** and **D**) at 6 months post-transplantation. The irregular bone structure and the gaps in the bone (arrows, **B**) worsened 6 months later (arrows, **E**). Narrowing of the fibula can also be seen over the 6 month period (**B** and **E**). Comparison of the cross-sectional tibial images at the start (**C**) and at the end (**F**) of the experiment show marked loss in trabecular architecture. TB indicates trabecular bone and CB indicates cortical bone. The images in A, B, D and E are shown at ~ 100% magnification, C and F are shown at ~ 290% magnification. Correlative images are all displayed using the same threshold values.

Table 1

Morphometric comparison of the tibia and femur from an engrafted osteogenesis imperfecta murine (*oim)* mouse before, 3- and 6-months post-transplantation (post-TP).

	Bone Vol./Total Vol.	Trabecular Thickness (mm)	Trabecular Number	Trabecular Spacing (mm)	Cortical Width (mm)	Trabecular Density (mg/ml)	Cortical Density (mg/ml)
Tibia							
Before TP	0.3881	0.0426	9.1077	0.0672	0.17	507.121	1420.709
3 months post-TP	0.4327	0.0442	9.7839	0.0576	0.21	682.412	1954.799
6 months post-TP	0.9991	0.0548	18.231	0.0052	0.25	746.645	2131.116
Femur							
Before TP	0.0894	0.0263	3.3941	0.2683	0.22	363.959	1248.670
3 months post-TP	0.1745	0.0314	5.5642	0.1484	0.24	518.617	1753.231
6 months post-TP	0.2196	0.0331	6.9806	0.1118	0.27	642.931	1805.032

Table 2

Morphometric comparison of tibia and femur from a control non-engrafted osteogenesis imperfecta murine (*oim)* mouse before and 6-months post-transplantation (post-TP).

	Bone Vol./Total Vol.	Trabecular Thickness (mm)	Trabecular Number	Trabecular Spacing (mm)	Cortical Width (mm)	Trabecular Density (mg/ml)	Cortical Density (mg/ml)
Tibia							
Before TP	0.5519	0.0536	10.2912	0.0435	0.18	560.108	1180.793
6 months post-TP	0.2822	0.0384	7.3576	0.0976	0.15	599.743	1216.236
Femur							
Before TP	0.1166	0.0355	3.2829	0.2691	0.21	590.475	832.458
6 months post-TP	0.0388	0.0192	2.0290	0.4737	0.14	509.985	900.972

Table 3

Morphometric comparison of tibia from an osteogenesis imperfecta murine (*oim)* mouse transplanted with BM cells enriched for HSCs (A) and a control *oim* mouse transplanted with *oim* BM cells (B) before, 3- and 6- months post-transplantation (post-TP).

	Bone Vol./Total Vol.	Trabecular Thickness (mm)	Trabecular Number	Trabecular Spacing (mm)	Cortical Width (mm)	Trabecular Density (mg/ml)	Cortical Density (mg/ml)
(A) Mouse transplanted with HSCs							
Before TP	0.2179	0.0322	6.9657	0.1123	0.13	653.75	1151.56
3 months post-TP	0.2806	0.0433	6.4870	0.1109	0.16	799.58	1095.32
6 months post-TP	0.2972	0.0443	6.7031	0.1049	0.18	831.62	1196.94
(B) Mouse transplanted with *oim* BM cells							
Before TP	0.2738	0.0369	7.4195	0.0979	0.15	690.96	1071.74
3 months post-TP	0.2311	0.0397	5.8277	0.1319	0.14	780.34	1122.7
6 months post-TP	0.1847	0.0443	4.1665	0.1957	0.12	806.65	1055.3